Three-sublattice mean-field approach for magnetoelectric coupling in multiferroics

Q. C. Li and J.-M. Liu*
Laboratory of Solid State Microstructures, Nanjing University, Nanjing 210093, China
and International Center for Materials Physics, Chinese Academy of Sciences, Shenyang, China
(Received 7 September 2006; revised manuscript received 14 December 2006; published 13 February 2007)

A three-sublattice mean-field approximation (MFA) to ferroelectromagnets with coexisting antiferromagnetic order and ferroelectric order is proposed to understand the magnetic transitions induced by magnetoelectric coupling between the two types of orders. The temperature dependence of magnetization, magnetic susceptibility and magnetoelectric susceptibility under different coupling strengths are calculated, indicating the intrinsic weak ferromagnetic transition at low temperature due to the magnetoelectric coupling. Comparing with the predictions given by earlier MFA, the present MFA predictions are in better accord with the Monte Carlo simulations.

DOI: 10.1103/PhysRevB.75.064415 PACS number(s): 77.80.Bh, 75.80.+q, 05.10.Ln

I. INTRODUCTION

Ferroelectromagnets (FEMs) are compounds in which magnetic and ferroelectric (or antiferroelectric) orders coexist below certain temperature. The interaction between the two types of orders, also called the magnetoelectric (ME) coupling, allows some additional features to the ferroelectric and magnetic transitions and introduces possible multifunctional responses of FEMs to external electric or magnetic field. For example, the fluctuations of ferroelectric polarization in response to external magnetic field and change of spin ordering to external electric field are usually expected. This unusual effect was first predicted in the phenomenological framework based on the symmetrical consideration. Cr_2O_3 was the first compound discovered to exhibit the ME effect,[1] subsequently, tens of FEMs were discovered and synthesized in the past decades, most of which are perovskite oxides.

In fact, the continuous interests in FEMs accumulated in the past decades can be found in the review papers of Smolenskii *et al.*,[2] Venevtsev *et al.*,[3] and Schmid.[4] Theoretically, Curie first pointed out the possibility of intrinsic ME behavior on the basis of symmetry considerations.[5] Decades later, Landau and Lifshitz proposed that the ME effects were only allowed in time-asymmetric systems.[6] They proposed a phenomenological theory including a free energy term in the form of $\alpha_{ij} \cdot H_i \cdot E_j$ where H_i is the magnetic field pointing to axis i, E_j is the electric field pointing to axis j and α_{ij} is the component of tensor $\boldsymbol{\alpha}$ designated as the linear ME effect. Meanwhile, theoretical works on microscopic origins of the ME response could be found in the papers of Rado,[7] Horneich *et al.*,[8] and Yatom *et al.*[9] In 1994, Gehring[10] summarized five possible mechanisms involved in the ME coupling, i.e., single-ion anisotropy, symmetric superexchange, antisymmetric superexchange, dipolar interactions, and Zeeman energy. For every mechanism, the magnetic interaction induced by an electric field and the consequences of different types of magnetic orders were discussed in detail.

For the microscopic theories mentioned above, the ME effect was considered as extrinsic. It is an induced magnetization that is absent before the electric field is applied. In 1994, an intrinsic ME coupling model which takes a full combination of electric and magnetic orders was proposed by Janssen.[11] Very recently it was proposed that in perovskite oxides the electric polarization is associated with the noncolinear spin configuration.[12,13] Taking into account these facts, the microscopic complexity of the ME coupling in FEMs remains to be a serious challenge, both experimentally and theoretically.

The present authors once performed a Monte Carlo (MC) simulation on the phenomenological model proposed by Janssen in a two-dimensional case and predicted a weak ferromagnetic (FM) transition induced by the ME coupling in a FEM with coexisting ferroelectric (FE)- antiferromagnetic (AFM) orders.[14,15] A mean-field approach (MFA) was also developed to understand the magnetic phase transitions and the ME coupling, in which the magnetic subsystem is partitioned into two sublattices. We hereafter call this MFA model as MFA2. However, the MFA2 model does not work well in the case of strong ME coupling strength, where remarkable discrepancies between the model calculations and MC simulations were found at low temperature (T) range. In particular, the weak FM transitions at low T cannot be correctly predicted by the MFA2 model. These disagreements suggest that the MFA2 model must to be reconsidered. In this work, we propose an improved MFA model (MFA3) for explaining the ME coupling between the FE order and magnetic order, aiming at reducing the discrepancies.

The remaining part of this work is organized as the following. In Sec. II, the Hamiltonian for a FEM lattice will be introduced briefly, followed by a description of the MFA2 model and the improved MFA3 model. We highlight the MC simulation procedure in Sec. III and then present in Sec. IV the details of the results of the MC simulations and calculations from MFA2 and MFA3 models, emphasizing the comparison between MFA2, MFA3, and MC simulation. Finally, a short summary will be given in Sec. V.

II. MODEL AND MEAN-FIELD APPROACHES

We consider a two-dimensional square FEM lattice with periodic boundary conditions. On each site are imposed two order parameters, i.e., the Ising spin s_i for magnetic interaction and electric displacement u_i for electric polarization. Ac-

cording to Janssen,[11,14,15] the Hamiltonian of such a FEM system includes the following three parts:

$$\tilde{H} = \tilde{H}^e + \tilde{H}^m + \tilde{H}^{me}, \tag{1}$$

where $\tilde{H}^e$, $\tilde{H}^m$, and $\tilde{H}^{me}$ represent the Hamiltonians of the electric subsystem, magnetic subsystem, and coupling term between the two subsystems, respectively.

We suppose that the electric polarization component of each site has an interaction with the background crystal, which can be described by a double-well potential as in the DIFFOUR (discrete frustrated φ^4) model. The Hamiltonian is given by

$$\tilde{H}^e = \sum_i \left(\frac{P_i^2}{2M} - \frac{A}{2}u_i^2 + \frac{B}{4}u_i^4 \right) - \sum_{\langle i,j \rangle} U_1 \cdot u_i u_j - \sum_i E \cdot u_i, \tag{2}$$

where $\langle i,j \rangle$ denotes the nearest neighbor, P_i is the momentum at site i, M is the mass, A and B are the double-well potential parameters, U_1 is the FE-interaction factor, and E is the electric field. For the magnetic subsystem, the interactions between spins s_i are described by the ANNNI (axial next-nearest neighbor Ising) model,

$$\tilde{H}^m = -\sum_{\langle i,j \rangle} J_1 \cdot s_i s_j - \sum_{[i,j]} J_2 \cdot s_i s_j - \sum_i H \cdot s_i. \tag{3}$$

By selecting parameters J_1 and J_2 properly, the magnetic subsystem may show an AFM or a FM phase transition. H in Eq. (3) is the magnetic field, and $[i,j]$ represents the next-nearest neighbor. In the strict sense, a two-dimensional lattice counted only with the nearest-neighbor Heisenberg exchange cannot sustain an AFM order. However, in this work, both the AFM coupling J_1 between the nearest neighbors and the FM coupling J_2 between the next-nearest neighbors are considered, which help to stabilize the AFM order in the two-dimensional case.

Electric polarization or electric field can cause a change in the magnitude of the symmetric exchange, which gives rise to the ME coupling effect. A possible form for such ME coupling is

$$\tilde{H}^{me} = -\sum_{\langle k,i \rangle, \langle k,j \rangle} \varepsilon_{i,j} \cdot g \cdot u_k^2 \cdot s_i s_j - \sum_{[i,j]} \varepsilon_{i,j} \cdot \kappa \cdot E \cdot s_i s_j, \tag{4}$$

where the first term is the coupling between the two subsystems (magnetic and electric), g is the coupling factor to scale the ME coupling strength. The second term is a symmetric two-ion exchange term taking into account the effect of the electric field on the magnetic order. Gehring[10] assumed that the variation of such a symmetric exchange is linearly proportional to the electric field. Factor κ in Eq. (4) is the proportional coefficient. Subscripts i, j in the first term of Eq. (4) denote the nearest neighbors of site k, but i and j refer to different sublattice sites. Here the magnetic subsystem should be partitioned into two magnetic sublattices, a and b. Parameter $\varepsilon_{i,j}$ is determined by magnetic sublattices to which s_i and s_j belong. $\varepsilon_{i,j}=1$ if both i and j belong to a sublattice; and $\varepsilon_{i,j}=-1$ if both belong to b sublattice, while $\varepsilon_{i,j}=0$ otherwise. We will show later that this two-sublattice partition of the magnetic subsystem, as employed in MFA2 model, is not reasonable when coupling factor g is large.

With the Hamiltonian defined by Eq. (1), one may study the phase transitions of the FEM lattice under different coupling factor g. We first highlight the MFA2 model for the ME coupling and then compare the MFA2 calculation with the MC simulation to be described below. Realizing that the ME coupling also has a weak effect on the FE order, we focus our interest on the magnetic properties.[15] Only the magnetic part [Eq. (3)] and ME coupling part [Eq. (4)] of the Hamiltonian [Eq. (1)] are considered in the MFA treatment. Following the standard procedure of molecular-field approach, we evaluate the equivalent magnetic field imposed on spin s_i as

$$-\frac{\partial \tilde{H}_m}{\partial s_i} = J_1 \sum_{\langle j \rangle} s_j + J_2 \sum_{[j]} s_j + H,$$

$$-\frac{\partial \tilde{H}_{me}}{\partial s_i} = \varepsilon \cdot g \cdot p^2 \sum_{[j]} s_j + \varepsilon \cdot \kappa \cdot E \sum_{[j]} s_j. \tag{5}$$

Applying the MFA treatment on Eq. (5) yields

$$-\frac{\partial \tilde{H}_m}{\partial s_i} = J_1 \cdot z_1 \cdot m + J_2 \cdot z_2 \cdot m + H,$$

$$-\frac{\partial \tilde{H}_{me}}{\partial s_i} = \varepsilon \cdot g \cdot p^2 \cdot z_2 \cdot m + \varepsilon \cdot \kappa \cdot E \cdot z_2 \cdot m, \tag{6}$$

where z_1 and z_2 denote, respectively, the numbers of the nearest-neighboring and next-nearest-neighboring sites, m and p take the configuration averaging of spin s_i and electric polarization moment u_i, respectively. Assuming that the system holds at the equilibrium state, m and p are in fact the order parameters of the magnetic and FE subsystems, respectively.

Considering the fact that the magnetic subsystem has an AFM ground state, it will be necessary to partition this subsystem into two equivalent magnetic sublattices a and b for the mean-field approach, although it will be shown below that this partition should be further modified. Thus, Eq. (6) can be rewritten as

$$-\left(\frac{\partial \tilde{H}_m}{\partial s_i}\right)_a = J_1 \cdot z_1 \cdot m_b + J_2 \cdot z_2 \cdot m_a + H,$$

$$-\left(\frac{\partial \tilde{H}_{me}}{\partial s_i}\right)_a = \varepsilon \cdot g \cdot p^2 \cdot z_2 \cdot m_a + \varepsilon \cdot \kappa \cdot E \cdot z_2 \cdot m_a,$$

$$-\left(\frac{\partial \tilde{H}_m}{\partial s_i}\right)_b = J_1 \cdot z_1 \cdot m_a + J_2 \cdot z_2 \cdot m_b + H,$$

$$-\left(\frac{\partial \tilde{H}_{me}}{\partial s_i}\right)_b = \varepsilon \cdot g \cdot p^2 \cdot z_2 \cdot m_b + \varepsilon \cdot \kappa \cdot E \cdot z_2 \cdot m_b. \tag{7}$$

From Eq. (7), one obtains the effective magnetic fields imposed on sublattices a and b, respectively,

$$H_a = H + J_1 \cdot z_1 \cdot m_b + z_2 \cdot [J_2 + (g \cdot p^2 + \kappa \cdot E)] \cdot m_a,$$

$$H_b = H + J_1 \cdot z_1 \cdot m_a + z_2 \cdot [J_2 - (g \cdot p^2 + \kappa \cdot E)] \cdot m_b. \quad (8)$$

Within the MFA framework, Hamiltonian Eq. (1) is thus simplified as

$$\tilde{H} = \tilde{H}^m + \tilde{H}^{me} = - H_a \cdot \sum_{ia} s_{ia} - H_b \cdot \sum_{ib} s_{ib}. \quad (9)$$

Given this simplified Hamiltonian, the ensemble averages in the partitioned magnetic subsystem under certain external magnetic field are given by

$$m_a = \tanh(\beta H_a), \quad s_{ia} = \pm 1,$$

$$m_b = \tanh(\beta H_b), \quad s_{ib} = \pm 1. \quad (10)$$

The magnetizations of the two sublattices, m_a and m_b, and the effective magnetic fields, H_a and H_b, can be calculated by numerically solving Eqs. (8) and (10) in the self-consistent manner. Hence, magnetization m, magnetic susceptibility χ_m, and magnetoelectric susceptibility χ_{me} for the whole lattice can be obtained,[15]

$$m = (m_a + m_b)/2,$$

$$\chi_m = \tfrac{1}{2}\beta \cdot [\mathrm{sech}^2(\beta H_a) + \mathrm{sech}^2(\beta H_b)],$$

$$\chi_{me} = \tfrac{1}{2} \cdot \kappa \cdot z_2 \cdot \beta [m_a \, \mathrm{sech}^2(\beta H_a) - m_b \, \mathrm{sech}^2(\beta H_b)], \quad (11)$$

where $\tanh(x)$ and $\mathrm{sech}(x)$ denote the hyperbolic functions.

It will be shown below that the values of m, χ_m, and χ_{me} as a function of T for different values of g, calculated by MFA2, exhibit significant discrepancies with those from the MC simulations if g is large (strong ME coupling). These discrepancies are attributed to the deficiency of the MFA2 developed above. Note that the first coupling term in Eq. (4) includes an effective AFM next-nearest-neighbor interaction on magnetic sublattice b. Therefore, a partition of the magnetic subsystem into two sublattices seems far from adequate. In particular, when factor g is large enough, antiparallel spin alignment in sublattice b may appear and thus this sublattice must be further partitioned. This explains why big discrepancies between the MC simulated results and the MFA2 predictions appear if the ME coupling becomes strong.

Noting the fact that the spin alignment in sublattice b may be AFM, it is necessary to partition sublattice b into two sublattices b_1 and b_2, in order to perform a MFA description of the FEM. In the present work, the new MFA is then developed based on the three-sublattice scheme (i.e., MFA3). Accordingly, a simple algorithm procedure produces,

$$H_a = H + \tfrac{1}{2} J_1 \cdot z_1 \cdot (m_{b1} + m_{b2}) + z_2 \cdot [J_2 + (g \cdot p^2 + \kappa \cdot E)] \cdot m_a,$$

$$H_{b1} = H + J_1 \cdot z_1 \cdot m_a + z_2 \cdot [J_2 - (g \cdot p^2 + \kappa \cdot E)] \cdot m_{b2},$$

$$H_{b2} = H + J_1 \cdot z_1 \cdot m_a + z_2 \cdot [J_2 - (g \cdot p^2 + \kappa \cdot E)] \cdot m_{b1}, \quad (12)$$

$$\tilde{H} = \tilde{H}^m + \tilde{H}^{me} = - H_a \cdot \sum_i s_{ia} - H_{b1} \cdot \sum_i s_{ib1} - H_{b2} \cdot \sum_i s_{ib2}, \quad (13)$$

$$m_a = \tanh(\beta H_a), \quad s_i = \pm 1,$$

$$m_{b1} = \tanh(\beta H_{b1}), \quad s_i = \pm 1,$$

$$m_{b2} = \tanh(\beta H_{b2}), \quad s_i = \pm 1, \quad (14)$$

$$m = \frac{1}{2}\left(m_a + \frac{(m_{b1} + m_{b2})}{2} \right),$$

$$\chi_m = \frac{\partial m}{\partial H} = \frac{1}{2}\beta \cdot \left(\mathrm{sech}^2(\beta H_a) + \frac{1}{2}[\mathrm{sech}^2(\beta H_{b1}) + \mathrm{sech}^2(\beta H_{b2})] \right),$$

$$\chi_{me} = \frac{1}{2} \cdot \kappa \cdot z_2 \cdot \beta \left(\langle s_a \rangle \mathrm{sech}^2(\beta H_a) - \frac{1}{2}[\langle s_{b2} \rangle \mathrm{sech}^2(\beta H_{b1}) + \langle s_{b1} \rangle \mathrm{sech}^2(\beta H_{b2})] \right), \quad (15)$$

where m_a, m_{b1}, m_{b2} and H_a, H_{b1}, H_{b2} can be calculated by self-consistently solving Eqs. (12)–(14). These equations are the replicas of Eqs. (8)–(11) of MFA2.

III. MONTE CARLO SIMULATION

In the next section, we shall present the evaluated m, χ_m, and χ_{me} as a function of T for different values of g from Eqs. (11)–(15) and from the MC simulations, respectively, in order to show the advantage of MFA3 over MFA2. It is assumed that the MC simulations are reliable and reflect the real ME coupling behaviors. Before presenting the results, we describe briefly the procedure of MC simulation and corresponding parameter evaluation.

For the MC sequences, the magnetic and FE order parameters can be evaluated by the following statistics:

$$m_i = \frac{1}{L^2} \sum_j^{L \times L} s_j,$$

$$p_i = \frac{1}{L^2} \sum_j^{L \times L} u_j,$$

$$S_i = \frac{1}{L^2} \sum_{[i,j]}^{L \times L} \varepsilon_{i,j} \cdot s_i s_j, \quad (16)$$

where m_i and p_i denote magnetization and electric polarization at arbitrary moment of the Markov sequence of the MC

TABLE I. Parameters selected for simulation ($T_N \ll T_E$).

Parameter	A	B	U_1	J_1	J_2	κ
Value	2	20	14	−0.2	0.2	1

simulation, S_i will be used for evaluating magnetoelectric susceptibility χ_{me}. The order parameters and susceptibilities of magnetic and electric subsystems are given below by configuration averaging,

$$m = \langle m_i \rangle,$$

$$p = \langle p_i \rangle,$$

$$\chi_m = \beta(\langle m_i^2 \rangle - \langle m_i \rangle^2),$$

$$\chi_p = \beta(\langle p_i^2 \rangle - \langle p_i \rangle^2), \tag{17}$$

where χ_p is the dielectric susceptibility of the lattice.

In fact, χ_{me} includes contribution from two parts. The first one comes from the fluctuation correlation between spins and electric dipoles, and the second from the two-ion term to the ME effect. Here we omit the first part since thermodynamically it is quite small compared to the second one

$$\chi_{me}^1 = \beta(\langle m_i \cdot p_i \rangle - \langle m_i \rangle \langle p_i \rangle),$$

$$\chi_{me}^2 = \beta(\langle m_i \cdot S_i \rangle - \langle m_i \rangle \langle S_i \rangle),$$

$$\chi_{me} \approx \chi_{me}^2. \tag{18}$$

Theoretically, a strong ME effect can be achieved in FE and FM materials. Nevertheless, most perovskite oxide FEMs are offered with the coexistence of FE ordering and AFM ordering due to the significant superexchange interactions. Therefore, it is of general significance to study the ME coupling in FE-AFM systems. Without losing the generality, the parameters of the system for calculations and simulations are given in Table I, which are chosen so that the Néel point T_N for the AFM order is lower than the Curie point T_E for the FE order ($T_N \ll T_E$), referring to most of the well studied FEMs like $Pb(Nb_{1/2}Fe_{1/2})O_3$, $BiFeO_3$, $YMnO_3$, etc.,[16–18] although the present model may not be applicable to these materials in any quantitative sense.

In the MC simulation, the size of the square lattice is $N = L^2$ where $L=24$. While the finite-size scaling effect was checked prior to the simulations, we do not pay special attention to the property very close to the transition point. At first, for every lattice site, spin s_i takes the value of 1 or −1 randomly and dipole u_i uniformly distributes over [−0.5, 0.5]. The spin-flip and dipole change are updated as follow: s_i or u_i are chosen randomly, then attempt to flip the spin or choose a random value for the dipole and calculate the change in system energy. At last, the lattice is updated to a new state following the Metropolis algorithm. We repeat this updating for every site and then finish one MC step (MCS). For every T, the first 50 000 MCS are discarded and the thermodynamic average is processed over the next 50 000–200 000 MCS.

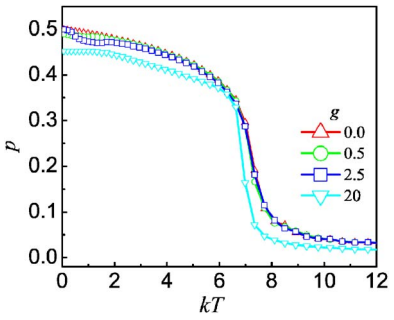

FIG. 1. (Color online) Dependence of electric polarization p as a function of temperature at different coupling factor g, as obtained by the MC simulation.

IV. RESULTS AND DISCUSSION

A. Monte Carlo simulations

The MC simulation shows that the lattice without ME coupling, i.e., $g=0$, consists of FE order and AFM order at $T \to 0$, with $kT_E \sim 7.3$ and $kT_N \sim 1.3$. When the ME coupling is introduced ($g>0$), the system will undergo a transition from AFM order to a weak FM order so long as the ME coupling is strong enough. The T dependences of m, χ_m, and χ_{me} upon different values of g are very similar with those reported in our previous work.[15] As mentioned above, the simulated p does not change much with varying g, as shown in Fig. 1. This fact allows us to safely compare the MFA calculations and MC simulations, where the simulated p-T data at $g=0$ are used for calculations from MFA2 and MFA3.

To understand the magnetic evolution for various g, a detailed investigation on the magnetizations of these three sublattices as a function of T will be proved helpful. We plot in Figs. 2(a)–2(e) the simulated magnetizations, m, m_a, m_b, m_{b1}, and m_{b2}, for the whole lattice and its three sublattices a, $b=b_1+b_2$, b_1, and b_2 under different values of g, respectively, noting $m=(m_a+m_b)/2$ and $m_b=(m_{b1}+m_{b2})/2$. At $g=0$, it is easy to learn that the system undergoes an AFM phase transition near $kT_N \sim 1.5$, consistent with the MC simulations. In this case, moments m_a, $m_b=(m_{b1}+m_{b2})/2$, m_{b1}, and m_{b2} all show a rapid rising as T goes down across T_N. The spins in sublattices b_1 and b_2 are in parallel alignment and their directions are opposite to spins in sublattice a, leading to $m=0$ at $T<T_N$. When factor g takes an intermediate value ($g=1.0$, cycle dots), upon decreasing T these sublattices show magnetization behaviors similar to those shown at $g=0$. The only and minor difference lies in that the magnitudes of m_{b1} and m_{b2} do not rise as rapidly as the case at $g=0$, leading to a small rising of m as a function of T below $kT=2.0$, which is again suppressed when T is close to zero. This corresponds to a weak FM regime, characterized by a small lump of the m-T relation, as shown in Fig. 2(a).

It is understood that for $g=0$, the AFM spin configuration for the lattice is favored by the AFM interactions ($-J_1 \cdot z_1 \cdot \langle i,j \rangle$) between the nearest neighbors and FM interactions ($-J_2 \cdot z_2 \cdot [i,j]$) between the next-nearest neighbors [Eq. (3)]. However, as $g>0$, the ME coupling term ($g \cdot z_2 \cdot p^2 \cdot [i,j]$) favors the AFM configuration between the next-nearest neighbors in b sublattice [Eq. (4)]. When

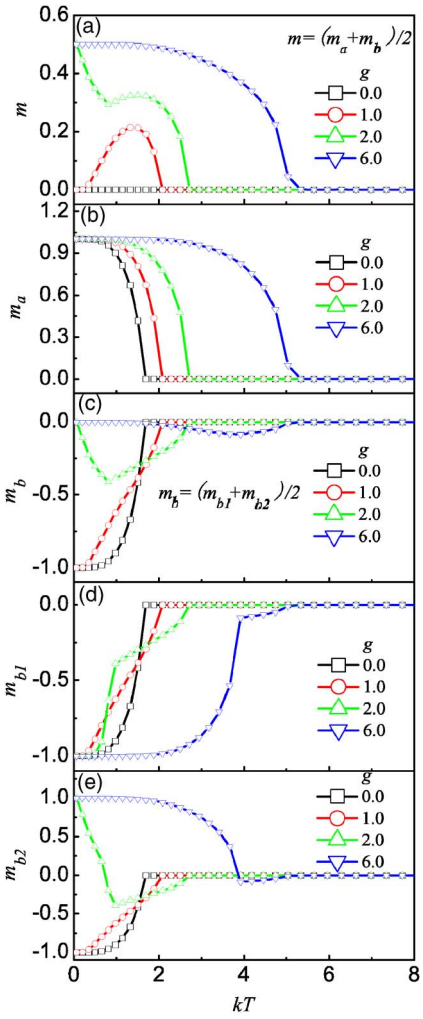

FIG. 2. (Color online) Temperature dependence of the magnetization in the whole lattice (a) and sublattice a (b), b (c), b_1 (d), and b_2 (e) at various g calculated by the three-sublattice MFA.

$-g\cdot z_2\cdot p^2 < J_1\cdot z_1 - J_2\cdot z_2$, spins of b sublattice may transform from the FM configuration to the AFM one, resulting in a weak FM transition of the whole lattice. Given the parameters in Table I, $p^2<0.25$ and $z_1=z_2=4$, $g>1.6$ is needed to induce the weak FM transition, in good agreement with the MFA calculations (both MFA2 and MFA3). As shown in Fig. 2, at $g=2$, the averaged magnetizations in sublattices a and b are still opposite to each other within the range of $kT=1.0-2.8$ because $m_a>0$ and $m_b<0$, but their magnitudes are different. Therefore, there is a net magnetization over the whole lattice. The underlying reason is that not all of the spins in sublattice b are aligned in parallel due to the strong ME coupling. Referring to Fig. 2(e), as $kT<kT_W\sim 1.0$, some spins in sublattice b_2 flip to the direction opposite to the spins in sublattice b_1. At $kT=0$, all spins in sublattice b_2 become antiparallel to those in sublattice b_1. Thus, $m_b=0$ at $kT=0$ and the system takes a weak FM ground state. When g increases further ($g=6.0$), spins in sublattice b_2 flip almost exactly below kT_N and hence the system starts to transfer into a weak FM phase instead of the AFM phase over the whole T range below kT_N. The increase of kT_N with increasing g is due to the enhancement of the effective magnetic interaction with increasing ME coupling.

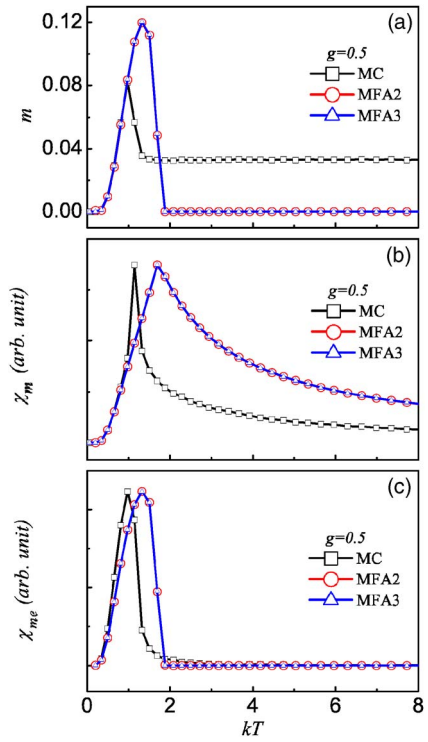

FIG. 3. (Color online) Temperature dependence of magnetization m (a), susceptibility χ_m (b), and magnetoelectric susceptibility χ_{me} (c) when $g=0.5$ by MC, two-sublattice MFA method (MFA2), and three-sublattice MFA method (MFA3).

B. Mean-field calculations and comparisons

Given the results of MC simulations, we present below the results calculated by MFA2 and MFA3 as well as their comparisons with the MC simulated results (MC). Three parameters, i.e., $m(T)$, $\chi_m(T)$, and $\chi_{me}(T)$ at different factor g will be presented for the comparisons. Figure 3 gives the calculated data from MFA2, MFA3, and MC simulated data in the case of weak ME coupling ($g=0.5$). It shows that $m(T)$, $\chi_m(T)$, and $\chi_{me}(T)$ calculated by MFA2 and MFA3 almost coincide with each other and all are in reasonable agreement in shape with the MC simulated ones except the slightly different peak positions and heights.

As factor g increases up to $g=2.5$, the MFA calculated and MC simulated results are presented in Fig. 4. The MFA2 seems not able to predict the FM ground state at $kT\sim 0$ where $m_a=1.0$ and $m_b=0$, while the MFA3 works much better and the FM ground state at $kT\sim 0$ is predicted. For the m-T relation [Fig. 4(a)], the MC simulation produces the two-step FM transitions. While the MFA2 can predict the high-T transitions, the low-T transition step cannot be reproduced, which is, however, reasonably predicted by the MFA3. In Figs. 4(b) and 4(c), the MC simulated two peaks of both $\chi_m(T)$ and $\chi_{me}(T)$, corresponding to the two-step transitions, can be reproduced roughly by the MFA3 while it cannot by the MFA2. This comparison indicates that the

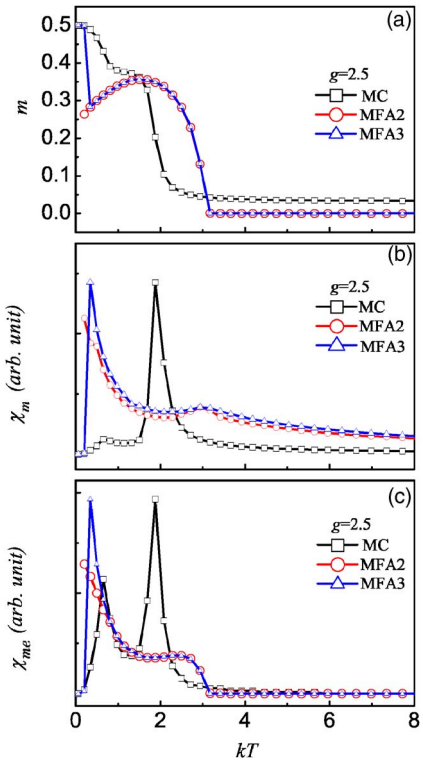

FIG. 4. (Color online) Temperature dependence of magnetization m (a), susceptibility χ_m (b), and magnetoelectric susceptibility χ_{me} (c) when $g=2.5$ by MC, MFA2, and MFA3.

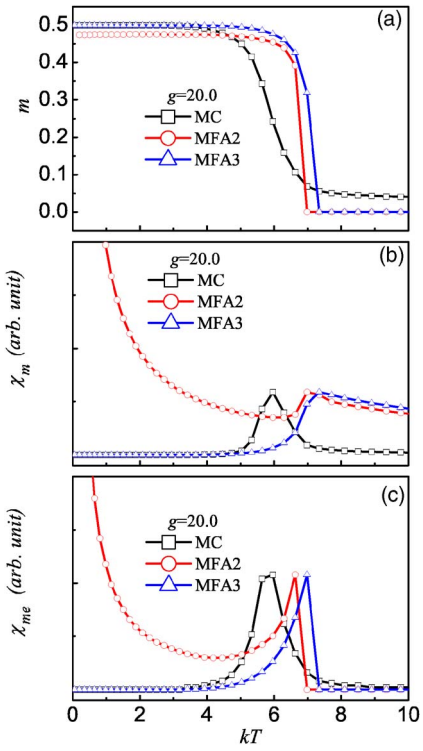

FIG. 5. (Color online) Temperature dependence of magnetization m (a), susceptibility χ_m (b), and magnetoelectric susceptibility χ_{me} (c) when $g=20.0$ by MC, MFA2, and MFA3.

MFA3 does work much better than the MFA2 in the qualitative sense. The advantage of the MFA3 over the MFA2 can be further demonstrated by the comparison at even larger g ($g=20$), as shown in Fig. 5. Because of the strong ME coupling, the FM transition point is shifted to the high-T side and no AFM transition is identified. In this case, the simulated m-T curve covering the FM transition regime can be reproduced by both the MFA2 and MFA3. However, the MFA2 predicts a divergence of both χ_m and χ_{me} at low-T limit, which is not true, as revealed by the MC simulation. The simulated χ_m-T and χ_{me}-T relations are well reproduced by the MFA3 calculation, in particular in the low-T range, in which we are interested.

To interpret the failure of the MFA2 at large coupling factor g, one may consult Eq. (7). For the MFA2, since the ME coupling induces an AFM arrangement in sublattice b, magnetization for this sublattice, m_b, is zero and its contribution to the effective magnetic field is considered to be zero. However, what should be mentioned is that each spin in sublattice b is surrounded by four antiparallel next-nearest neighbors and the effective magnetic field imposed on it is nonzero. By further partitioning sublattice b into two sublattices, the above difficulty is partially overcome. As shown by Eq. (12), the MFA3 gives a reasonable prediction of the effective field imposed on each spin in sublattices a, b_1, and b_2. Consequently, $m(T)$, $\chi_m(T)$, and $\chi_{me}(T)$ calculated by the MFA3 are in better agreement with the MC simulated data than those calculated by the MFA2.

C. Discussion and remarks

Despite the improvement achieved by the MFA3, there are still remarkable differences between the MC simulations and the MFA calculations in the quantitative sense, for instance the inconsistency of the peak height of $\chi_m(T)$ and $\chi_{me}(T)$ curves shown in Fig. 4. One of the reasons is probably that the values p used for the MFA calculation is assumed to be independent of coupling factor g. Especially, the small slump in the p-T curve near $kT=1.0$ at $g=2.5$, which is not available at $g=0$, may probably contribute to the discrepancies between the simulated and MFA3 calculated data (shown in Fig. 4 for $g=2.5$). Nevertheless, the assumption of independence of p on g seems to be reasonable, because the dependence of p on g is not significant, as shown in Fig. 1. Even so, we recalculate the χ_m-T and χ_{me}-T curves by the MFA3 using the simulated p-T data at $g=2.5$ (open squares in Fig. 1), and the results are presented in Fig. 6 labeled by MFA3*. By comparing with the data at $g=0$ (shown in Fig. 4), it is observed that taking the weak dependence of p on g does affect the calculated parameters χ_m and χ_{me} as a function of T at low-T range, but no essential reduction of the discrepancies between the MC simulated results and the MFA3 calculated ones is identified. Another possible reason for the discrepancies is that the MC simulation is performed on a finite size lattice. Hence the simulated results might deviate slightly from those on an infinite lattice. Nevertheless, such a finite-size effect is not significant, as revealed by our preliminary simulation, although our limited computa-

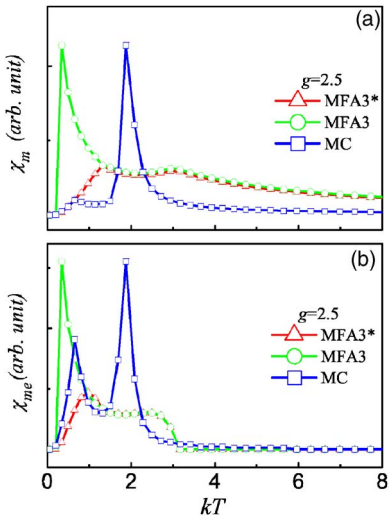

FIG. 6. (Color online) Comparison of susceptibility χ_m (a) and magnetoelectric susceptibility χ_{me} (b) at $g=2.5$ between the MFA3 calculations based on the MC simulated p-kT relations at $g=0.0$ (labeled as MFA3) and on the MC simulated p-kT relation at $g=2.5$ (labeled as MFA3*). The MC simulated χ_m-kT and χ_{me}-kT data at $g=2.5$ are also presented for comparison.

tional capability restrains us from checking in detail the finite-size effect. Besides, spin wave in the magnetic subsystem, which is certainly one ingredient of the magnetoelectric physics, might contribute to the discrepancies too, especially at low T range and near the transition points. Unfortunately, spin wave behaviors with FEM lattices seem to be a challenging issue and a comprehensive approach to its effect in FEM systems is still going on.

V. CONCLUSION

In conclusion, we have developed a mean-field approach based on a three-sublattice-partition on two-dimensional FE-AFM ferroelectromagnets. The magnetic properties and ME coupling effect calculated by this mean-field approach are compared with the MC simulations and the two-sublattice mean-field approach developed earlier.[15] As a result, the weak ferromagnetic transition at low temperature has been successfully predicted and the qualitative discrepancies between the approach and MC simulations have been repaired, although the quantitative differences between them remain to be handled. This mean-field approach provides us with a deeper understanding of the complicated spin configurations and phase transitions in ferroelectromagets of FE and AFM orders.

ACKNOWLEDGMENTS

The authors thank the Natural Science Foundation of China (Grants Nos. 50332020 and 10021001) and National Key Projects for Basic Research of China (Grants Nos. 2002CB613303 and 2006CB921802).

*Corresponding author; Electronic address: liujm@nju.edu.cn

[1] I. E. Dzyaloshinskii, Sov. Phys. JETP **10**, 628 (1959).
[2] G. A. Smolenskii and I. E. Chupis, Sov. Phys. Usp. **25**, 475 (1982).
[3] Y. N. Venevtsev and V. V. Gagulin, Ferroelectrics **162**, 23 (1994).
[4] H. Schmid, Ferroelectrics **161**, 1 (1994).
[5] P. Curie, J. Phys. Theor. Appl. **3**, 393 (1894).
[6] L. D. Landau and E. M. Lifshitz, *Electrodynamics of Continuous Media* (Addison-Wesley, Reading, MA, 1960).
[7] G. T. Rado, Phys. Rev. Lett. **6**, 609 (1961); Phys. Rev. **128**, 2546 (1965).
[8] R. M. Hornreich and S. Shtrikman, Phys. Rev. **161**, 506 (1967).
[9] H. Yatom and R. Englman, Phys. Rev. **188**, 793 (1969); **188**, 803 (1969).
[10] G. A. Gehring, Ferroelectrics **161**, 275 (1994).
[11] T. Janssen, Ferroelectrics **162**, 265 (1994).
[12] H. Katsura, N. Nagaosa, and A. V. Balatsky, Phys. Rev. Lett. **95**, 057205 (2005).
[13] Y. Yamasaki, S. Miyasaka, Y. Kaneko, J.-P. He, T. Arima, and Y. Tokura, Phys. Rev. Lett. **96**, 207204 (2006).
[14] X. S. Gao, J.-M. Liu, X. Y. Chen, and Z. G. Liu, J. Appl. Phys. **88**, 4250 (2000).
[15] J.-M. Liu, Q. C. Li, X. S. Gao, Y. Yang, X. H. Zhou, X. Y. Chen, and Z. G. Liu, Phys. Rev. B **66**, 054416 (2002).
[16] Y. N. Venevtsev, V. V. Gagulin, and I. D. Zhitomirsky, Ferroelectrics **73**, 221 (1987).
[17] S. V. Kizelev, R. P. Ozerov, and G. S. Zhdanov, Sov. Phys. Dokl. **145**, 1255 (1962).
[18] G. A. Smolenskii and V. A. Bokov, J. Appl. Phys. **35**, 915 (1964).